Measurement of the Cell−Substrate Separation and the Projected Area of an Individual Adherent Cell Using Electric Cell−Substrate Impedance Sensing

Pahnit Seriburi,* Shawn McGuire, Ashutosh Shastry, Karl F. Böhringer, and Deirdre R. Meldrum

Microscale Life Sciences Center, University of Washington, Seattle, Washington 98195

This work presents an electrical technique called electric cell−substrate impedance sensing to measure the cell−substrate separation and the projected area of an individual adherent cell. Cell adhesion and cell spreading are fundamental processes of adherent cells. By recording changes in the cell−substrate separation, the projected area, or both properties with time, the dynamics of cell spreading and cell adhesion can be studied. The advantage of this electrical technique is that it enables a measurement of many individual cells simultaneously. This is a great benefit to the study of heterogeneity in cell populations. The research consisted of building a custom impedance sensing setup, designing an in vitro assay to record an impedance spectrum of an individual living cell, and developing a data analysis method to obtain two properties of the cell from curve-fitting of the impedance spectrum. The values of the cell−substrate separation and the projected area of an individual cell were within the expected ranges and in agreement with those obtained from optical microscopy.

Cell adhesion and cell spreading are fundamental processes of adherent cells, crucial to the body's defense system,[1–3] the formation of tissues,[4] and the signal transduction pathways of a cell.[5,6] Due to the complexity of cell adhesion and cell spreading processes, these cellular processes have been studied at many levels including the tissue, individual cell, and molecular levels.

At the individual cell level, several properties of a cell have been associated with cell adhesion and cell spreading processes. Changes in the cell−substrate separation and the projected area of an individual cell simultaneously occur when cells spread and when cells adhere. Thus, by recording changes in the cell−substrate separation, the projected area, or both properties with time, the dynamics of cell spreading and cell adhesion can been studied.[2,7–10] Still, little is known about how these two properties influence other cellular processes and how their values are influenced by the interaction between the cell and the substrate. Evidence in the literature reveals some of these correlations. For example, the survival rate of individual cells increases when a cell is given more surface area to spread out (or the larger the projected area).[11] Also, the increase in the projected area of an individual spreading cell influences the level of Ca^{2+} in the cell nucleus.[12] For the cell−substrate separation, individual astrocytes exhibit different values of cell−substrate separations when subjected to laminin and fibronectin.[13] The increase in the cell−substrate separation of endothelial cells may be closely linked to the decrease in how tightly the cells adhere to the substrate.[8]

Conventionally, the cell−substrate separation and the projected area of an individual cell are measured using a variety of optical methods.[1,2,10–16] Electrical methods offer a simpler and more cost-effective technique than optical methods to measure many individual cells at the same time. Measuring many individual cells simultaneously allows the study of variability among cells in the populations (heterogeneity in cell populations), which is the subject of increasing interest in recent years.[17–19] Studying heterogeneity will lead to a better understanding of stem cells as well as diseases such as cancer where phenotypically variable cells

* To whom correspondence should be addressed. Address: 616 NE Northlake Place, Room 440, Seattle, WA 98105. Phone: (206) 616-2570. Fax: (206) 616-5721. E-mail: pahnit@u.washington.edu.

(1) Fleire, S. J.; Goldman, J. P.; Carrasco, Y. R.; Weber, M.; Bray, D.; Batista, F. D. *Science* **2006**, *312*, 738–741.
(2) Sengupta, K.; Aranda-Espinoza, H.; Smith, L.; Janmey, P.; Hammer, D. *Biophys. J.* **2006**, *91*, 4638–4648.
(3) Imhof, B. A.; Aurrand-Lions, M. *Nat. Rev. Immunol.* **2004**, *4*, 432–444.
(4) Gumbiner, B. M. *Cell* **1996**, *84*, 345–357.
(5) Geiger, B.; Bershadsky, A.; Pankov, R.; Yamada, K. M. *Nat. Rev. Mol. Cell Biol.* **2001**, *2*, 793–805.
(6) Giancotti, F. G.; Ruoslahti, E. *Science* **1999**, *285*, 1028–1032.
(7) Chamaraux, F.; Fache, S.; Bruckert, F.; Fourcade, B. *Phys. Rev. Lett.* **2005**, *94*, 158102.
(8) Kataoka, N.; Iwaki, K.; Hashimoto, K.; Mochizuki, S.; Ogasawara, Y.; Sato, M.; Tsujioka, K.; Kajiya, F. *Proc. Natl. Acad. Sci. U.S.A.* **2002**, *99*, 15638–15643.
(9) Lo, C.-M.; Ferrier, J. *Eur. Biophys. J.* **1999**, *28*, 112–118.
(10) Lotz, M. M.; Burdsal, C. A.; Erickson, H. P.; McClay, D. R. *J. Cell. Biol.* **1989**, *109*, 1795–1805.
(11) Chen, C. S.; Mrksich, M.; Huang, S.; Whitesides, G. M.; Ingber, D. E. *Science* **1997**, *276*, 1425–1428.
(12) Itano, N.; Okamoto, S.-i.; Zhang, D.; Lipton, S. A.; Ruoslahti, E. *Proc. Natl. Acad. Sci. U.S.A.* **2003**, *100*, 5181–5186.
(13) Braun, D.; Fromherz, P. *Phys. Rev. Lett.* **1998**, *81*, 5241–5244.
(14) Giebel, K.-F.; Bechinger, C.; Herminghaus, S.; Riedel, M.; Leiderer, P.; Weiland, U.; Bastmeyer, M. *Biophys. J.* **1999**, *76*, 509–516.
(15) Burmeister, J. S.; Olivier, L. A.; Reichert, W. M.; Truskey, G. A. *Biomaterials* **1998**, *19*, 307–325.
(16) Davies, P. F.; Robotewskyj, A.; Melvin, L. G. *J. Clin. Invest.* **1993**, *91*, 2640–2652.
(17) Carlo, D. D.; Lee, L. P. *Anal. Chem.* **2006**, *78*, 7918–7925.
(18) Cohen, J. TR10: Single-Cell Analysis. *Technology Review*. http://www.technologyreview.com (accessed Nov 16, 2007).
(19) Lidstrom, M. E.; Meldrum, D. R. *Nat. Rev. Microbiol.* **2003**, *1*, 158–164.

10.1021/ac800036c CCC: $40.75 © XXXX American Chemical Society
Published on Web 04/11/2008

have been observed.[20,21] A few electrical methods such as a transistor probe[22] and impedance sensing using microelectrodes[23,24] have been previously used to study attachment of individual adherent cells. However, none of these techniques aim at providing both the cell−substrate separation and the projected area of an individual cell in the same measurement. This work evaluates another electrical method called electric cell−substrate impedance sensing (ECIS) that has been used as a tool to study properties of monolayers of cells for many years.[25–27] In our view, the ECIS technique has the ability to measure both the cell−substrate separation as well as the projected area of an individual cell simultaneously, and the technique can be easily scaled up for measurements of many individual cells at the same time.[28]

This present study demonstrates the first measurement of the cell−substrate separation and the projected area of an individual cell using the ECIS technique. A custom impedance sensing setup has been built to accommodate additional features that are not available in the conventional ECIS setup. An in vitro assay has been designed for using this setup to record an impedance spectrum of an individual living cell. A data analysis method has been developed to obtain two properties of the cell from the impedance spectrum. The results provide an important step toward studying heterogeneity in cell spreading and cell adhesion processes at the individual cell level.

EXPERIMENTAL SECTION

Cell Culture and Reagents. Keratinocytes from an individual with junctional epidermolysis bullosa gravis form (JEBG cells) were maintained at 37 °C under a humidified 5% CO_2 atmosphere. The culture medium was KGM-Keratinocyte medium supplemented with growth factors, cytokines, and supplements (Lonza, Walkersville, MD). JEBG cells were selected because they were adherent, autonomous, and simple to culture.

Device and Instrumentation. We designed the dimensions and layout of the electrodes in the ECIS device used in this study. The customized ECIS device was obtained from Applied Biophysics, Inc. (ABP) (Troy, NY). Previous work provided an optical image of the ECIS device.[29] Each ECIS device had eight wells with one gold electrode pair at the bottom of each well. Each electrode pair had one square counter electrode (area = 1.5 mm × 8 mm = 120 mm^2) and one round microelectrode (area = $A_{microelectrode} = \pi(15\,\mu m)^2 = 706\,\mu m^2$) that was located in the middle of the circular gold lead. The area boundaries of both electrodes were defined by patterning a photoresist using standard photolithography. The thickness of the gold was 50 nm, permitting optical transparency by unaided visual examination.

An impedance at multiple frequencies, i.e., an impedance spectrum ($Z(\omega)$ where ω is frequency) across the electrode pair was measured using a 4294A impedance analyzer (Agilent, Santa Clara, CA). A sinusoidal voltage was applied across the electrode pair with an amplitude of 25 mV (peak to peak) and a frequency ranging between 10 kHz and 1 MHz at 201 incrementally fixed values of frequency. An optical image of the microelectrode was also acquired from underneath the well using a LU055 USB camera (Lumenera, North Andover, MA) equipped with a 40× DIN objective (Edmund Optics, Barrington, NJ). A red Luxeon Star/O LED (Lumileds, San Jose, CA) was fixed above the well and turned on for 400 ms for each exposure of an image. An impedance analyzer, a USB camera, and a LED on/off switch were all controlled automatically via a custom software program called *Capture*. *Capture* permitted users to obtain a series of data sets ($Z(\omega)$ and the corresponding optical image) with adjustable time intervals between individual data sets.

ECIS Assay for an Individual Cell. The night before each experiment, one well of the ECIS device was filled with 400 μL of supplemented KGM and the device was moved into an incubator that was maintained at 37 °C under a humidified 5% CO_2 atmosphere. This step was recommended by ABP to allow the ECIS device to release any small molecules left on the surface of gold electrodes into the medium to yield more repeatable measurements.

On the day of the experiment, a cell suspension with a concentration of 5×10^5 cells/mL was prepared and 50 μL of the cell suspension (approximately 2.5×10^4 cells) was added to the well of the ECIS device. This step was done as quickly as possible to minimize the fluctuation of temperature and CO_2 level in the incubator due to the opening and closing of the incubator door. For each data set, $Z(\omega)$ across the electrode pair was recorded in the form of magnitude (Mag$Z(\omega)$) and phase (Phase$Z(\omega)$), and an optical image of the microelectrode with or without an individual cell was simultaneously acquired. The time interval between two individual data sets was set to 1 min. The experiment was terminated after 1−2 days or when sufficient data sets were obtained.

Data Analysis: Image Processing and the Fitting of $Z(\omega)$. For each series of data sets recorded in one experiment, only the data set with its optical image showing a microelectrode with an individual cell was selected. $Z(\omega)$ of that data set was called $Z_{cell}(\omega)$. With the use of the free software package, *ImageJ*,[30] the projected area of the individual cell of that data set was calculated by manually selecting the subregion of the corresponding optical image that belonged to the individual cell. This processing of images was mainly for the purpose of comparison of the results from ECIS measurement with those obtained from optical measurement.

The cell−substrate separation (h) and the projected area (A_{cell}) of the individual cell were obtained by fitting $Z_{cell}(\omega)$ to a model function ($Z(\omega, h, A_{cell})$) containing both properties as parameters of interest. The fit was achieved by minimizing an objective function (S) with respect to h and A_{cell} using the Nelder−Mead method.[31] S is defined as

(20) Reya, T.; Morrison, S. J.; Clarke, M. F.; Weissman, I. L. *Nature* **2001**, *414*, 105–111.
(21) Pardal, R.; Clarke, M. F.; Morrison, S. *J. Nat. Rev. Cancer* **2003**, *3*, 895–902.
(22) Kiessling, V.; Müller, B.; Fromherz, P. *Langmuir* **2000**, *16*, 3517–3521.
(23) Borkholder, D. A. Ph.D. thesis, Stanford University, Palo Alto, CA, 1998.
(24) Lind, R.; Connolly, P.; Wilkinson, C. D. W.; Breckenridge, L. J.; Dow, J. A. T. *Biosens. Bioelectron.* **1991**, *6*, 359–367.
(25) Welcome to Applied BioPhysics site. http://www.biophysics.com (accessed Nov 17, 2007).
(26) Giaever, I.; Keese, C. R. *Nature* **1993**, *366*, 591–592.
(27) Giaever, I.; Keese, C. R. *Proc. Natl. Acad. Sci. U.S.A.* **1991**, *88*, 7896–7900.
(28) Huang, X.; Nausieda, I.; Greve, D. W.; Domach, M. M.; Nguyen, D. *Proc. IEEE Sensors* **2004**, *1*, 72–75.
(29) Seriburi, P.; Shastry, A.; Ren, T.; Gales, S.; Böhringer, K. F.; Meldrum, D. *Solid-State Sensors Actuators and Microsystems Conferences* **2007**, 469–472.
(30) Abramoff, M. D.; Magelhaes, P. J.; Ram, S. J. *Biophotonics Int.* **2004**, *11*, 36–42.

$$S=\sum_{i=1}^{201}\left\{\left[\frac{\mathrm{Mag}Z_{\mathrm{cell}}(\omega_i)-\mathrm{Mag}Z(\omega_i,h,A_{\mathrm{cell}})}{\mathrm{Mag}Z(\omega_i,h,A_{\mathrm{cell}})}\right]^2+\left[\frac{\mathrm{Phase}Z_{\mathrm{cell}}(\omega_i)-\mathrm{Phase}Z(\omega_i,h,A_{\mathrm{cell}})}{\mathrm{Phase}Z(\omega_i,h,A_{\mathrm{cell}})}\right]^2\right\} \quad (1)$$

where i is number of fixed values of frequency. The Nelder−Mead method was implemented using the fminsearch function in *MATLAB* where S was the function to be minimized (fun) and the initial estimate of h and A_{cell} was the starting vector (x_0). Although the Nelder−Mead method was a robust fit technique, sometimes the search would encounter a local minimum before reaching the absolute minimum.[32] To ensure that S was the global minimum for each $Z_{\mathrm{cell}}(\omega)$ in these data sets, the minimization program was run using three values of x_0; [500 nm and 200 μm^2], [100 nm and 200 μm^2], and [1000 nm and 200 μm^2] and h and A_{cell} that were obtained from the run with the lowest S were selected. These final values of h and A_{cell} obtained from Nelder−Mead method were compared with those obtained from the brute force method, and they were in agreement.

An equivalent circuit model $Z(\omega, h, A_{\mathrm{cell}})$ was used to approximate $Z_{\mathrm{cell}}(\omega)$. $Z(\omega, h, A_{\mathrm{cell}})$ is defined as

$$Z(\omega,\ h,\ A_{\mathrm{cell}})=((Z_{\mathrm{c}}\,||\,Z_{\mathrm{nc}})+R_{\mathrm{s}})\,||\,(C_{\mathrm{para}}+R_{\mathrm{para}})\,||\,C_{\mathrm{wire}} \quad (2)$$

where Z_{c} is the impedance of microelectrode covered by an individual cell, Z_{nc} is the impedance of a microelectrode not covered by a cell, R_{s} is the resistance of the cell medium between the microelectrode and the counter electrode, C_{para} is the capacitance of the photoresist deposited on the circular gold lead, R_{para} is the resistance of the cell medium between the circular gold lead and the counter electrode, and C_{wire} is a leakage capacitance of leads connecting the electrode pair to the measurement terminal of the impedance analyzer.

Z_{c} was modeled by modifying a model of the specific impedance for a cell-covered electrode developed by Giaever and Keese (G&K model).[27] R_{b} in the G&K model was set to zero because there were no other cells besides the cell of interest and the cell was thin. Then, the specific impedance was divided by A_{cell} to obtain Z_{c} (unit of Ω). Therefore, Z_{c} is defined as

$$Z_{\mathrm{c}}(\omega)=\frac{\dfrac{Z_{\mathrm{m}}(\omega)+Z_{\mathrm{n}}(\omega)}{A_{\mathrm{cell}}}}{1+\dfrac{2Z_m(\omega)I_1(\gamma(\omega)r_{\mathrm{c}})}{\gamma(\omega)r_{\mathrm{c}}Z_{\mathrm{n}}(\omega)\,I_0(\gamma(\omega)r_{\mathrm{c}})}} \quad (3)$$

where Z_{m} is the specific impedance of the cell, Z_{n} is the specific impedance of the electrode−electrolyte interface, r_{c} is the radius of the cell, and I_0 and I_1 are the modified Bessel functions of the first kind of order 0 and 1, respectively. Note that Z_{c} is a function of ω because Z_{m}, Z_{n}, and γ are a function of ω. γ is defined[27] as

$$\gamma(\omega)=\sqrt{\frac{\rho\left(\dfrac{1}{Z_{\mathrm{n}}(\omega)}+\dfrac{1}{Z_{\mathrm{m}}(\omega)}\right)}{h}} \quad (4)$$

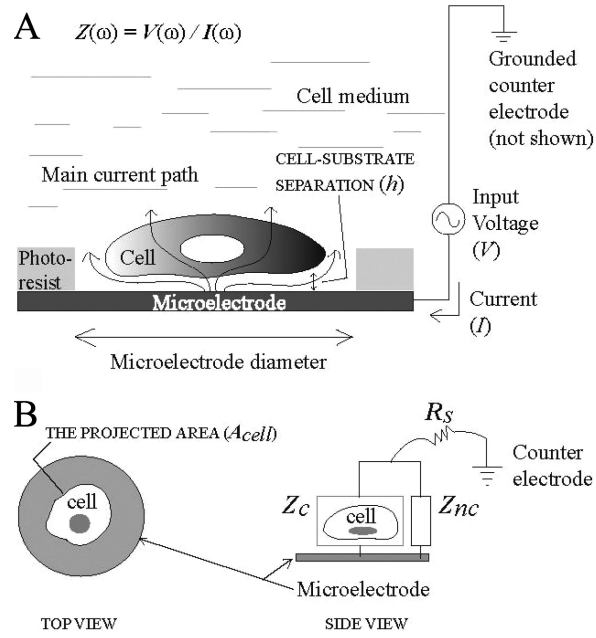

Figure 1. (A) Schematic view of the ECIS technique for measuring h and A_{cell}. A cell was seeded on the microelectrode submerged in cell medium, and $Z(\omega)$ was measured across the electrode pair. h and A_{cell} determine the values of $Z(\omega)$ because they restrict how much current ($I(\omega)$) can be obtained at a given applied voltage ($V(\omega)$) in the ECIS measurement. (B) The schematic view of three circuit elements of the equivalent circuit model representing the impedance of the main current path.

where ρ is the resistivity of the cell medium. Z_{m} is defined[33] as

$$Z_{\mathrm{m}}(\omega)=\frac{2}{\dfrac{1}{R_{\mathrm{m}}}+j\omega C_{\mathrm{m}}} \quad (5)$$

where j is $\sqrt{-1}$ and R_{m} and C_{m} are the specific resistance and capacitance of the cell plasma membrane, respectively. Z_{n} could be described by many models,[34–36] but Z_{n} in this setup was best represented using the constant-phase element. Z_{n} is defined[34] as

$$Z_{\mathrm{n}}(\omega)=\frac{1}{(j\omega)^{\alpha}C_{\mathrm{i}}} \quad (6)$$

where C_{i} is a specific capacitance of the electrode−electrolyte interface and α is a constant ($0 \le \alpha \le 1$).

Z_{nc} was modeled by dividing Z_{n} by the area of the microelectrode without the cell. This area is the difference between $A_{\mathrm{microelectrode}}$ and A_{cell}. Thus, Z_{nc} is defined as

$$Z_{\mathrm{nc}}(\omega)=\frac{Z_{\mathrm{n}}(\omega)}{A_{\mathrm{microelectrode}}-A_{\mathrm{cell}}} \quad (7)$$

(31) Nelder, J. A.; Mead, R. *Comput. J.* **1965**, *7*, 308–313.
(32) Boukamp, B. A. *Solid State Ionics* **2004**, *169*, 65–73.
(33) Bodmer, J. E.; English, A.; Brady, M.; Blackwell, K.; Haxhinasto, K.; Fotedar, S.; Borgman, K.; Bai, E.-W.; Moy, A. B. *Am. J. Physiol. Cell Physiol.* **2005**, *289*, 735–747.
(34) Tlili, C.; Reybier, K.; Gèloën, A.; Ponsonnet, L.; Martelet, C.; Ouada, H. B.; Lagarde, M.; Jaffrezic-Renault, N. *Anal. Chem.* **2003**, *75*, 3340–3344.
(35) Franks, W.; Schenker, I.; Schmutz, P.; Hierlemann, A. *IEEE Trans. Biomed. Eng.* **2005**, *52*, 1295–1302.
(36) Kovacs, G. T. A. Introduction to the Theory, Design, and Modeling of Thin-Film Microelectrodes for Neural Interfaces. In *Enabling Technologies for Cultured Neural Networks*; Stenger, D. A., McKenna, T., Eds.; Academic Press: London, 1994; pp 121−166.

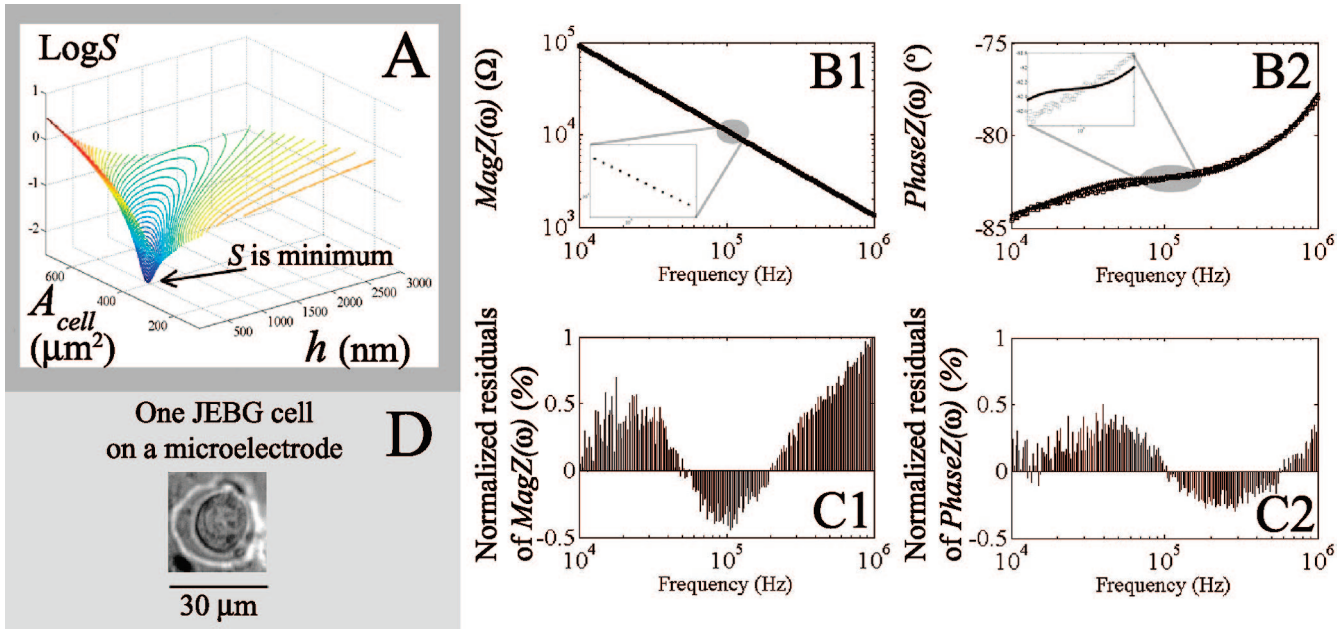

Figure 2. (A) 3D contour plot of S for a given pair of h and A_{cell}. The global minimum of S was obtained from this data set. Comparison of (B1) magnitude and (B2) phase between $Z_{cell}(\omega)$ (□) and the best-fit impedance spectrum (•) over the range of frequency. (C) The normalized residuals (both magnitude and phase) representing the quality of fitting were calculated. (D) The corresponding optical image in this data set showing a microelectrode with one individual cell.

Z_{nc} was arranged in parallel with Z_c because the current leaving the microelectrode would either go through the cell via Z_c or go around the cell via Z_{nc} (Figure 1B).

Equations 3–6 show that Z_c is a function of five properties of an individual cell (A_{cell}, r_c, h, R_m, and C_m). For the purpose of this study, however, only two properties of the cell (h and A_{cell}) were obtained from curve fitting $Z_{cell}(\omega)$ because they were relevant to the study of cell adhesion and cell spreading. R_m and C_m were assumed constant for a particular type of cells and did not change during the experiment, and r_c was approximated using A_{cell} ($r_c = [A_{cell}/\pi]^{1/2}$) based on the assumption that the shape of the cell was round.

From eqs 2–7, $Z(\omega, h, A_{cell})$ is function of 14 variables (A_{cell}, r_c, h, R_m, C_m, C_{wire}, ω, $A_{microelectrode}$, ρ, R_s, R_{para}, C_{para}, C_i, and α) or 12 variables when we approximated $r_c = [A_{cell}/\pi]^{1/2}$ and $\rho = R_s 4[A_{microelectrode}/\pi]^{1/2}$.[23,36] However, besides h and A_{cell}, most of the variables were known. R_m and C_m of JEBG cells were approximated to 0.1 $\Omega \cdot m^2$ and 0.0153 F/m ^{2}, respectively.[37,38] C_{wire} was obtained by measuring $Z(\omega)$ across an electrode pair in an empty ECIS well. The measured $Z(\omega)$ suggested that C_{wire} could be represented as an ideal capacitance with a value of 1 pF. The range of ω was set to 10 kHz to 1 MHz, the same as the frequency range used in the actual measurement. $A_{microelectrode}$ was measured using *ImageJ*. R_s, R_{para}, C_{para}, C_i, and α were obtained by curve fitting $Z(\omega)$ of the data set with its optical image showing a microelectrode without cell, i.e., $Z_{nocell}(\omega)$ to a model containing these five variables ($Z(\omega, R_s, R_{para}, C_{para}, C_i, \alpha)$). This model was the special case of the equivalent circuit model presented in eq 2 when $Z_c = 0$ and $A_{cell} = 0$. $Z(\omega, R_s, R_{para}, C_{para}, C_i, \alpha)$ is defined as

$$Z(\omega, R_s, R_{para}, C_{para}, C_i, \alpha) = (Z_{nc} + R_s) \,||\, (C_{para} + R_{para}) \,||\, C_{wire} \quad (8)$$

There were many $Z_{nocell}(\omega)$ in each series of data sets measured in one experiment. $Z_{nocell}(\omega)$ that was recorded at a time close to that of $Z_{cell}(\omega)$ was selected for obtaining five variables to be used in the extraction of h and A_{cell}.

Measurement of *h* Using Transmission Electron Microscopy (TEM). TEM was used to qualitatively approximate h for the purpose of comparison of the results from ECIS measurement with those obtained from optical measurement. For TEM, an ECIS device with JEBG cells grown to confluency at the bottom of each well was prepared. The cells were fixed in half-strength Karnovsky's fixative (2.0% paraformaldehyde, 2.5% glutaraldehyde, 0.1 M cacodylate buffer, 3 mM $CaCl_2$, pH 7.3), postfixed in 1.0% OsO_4, en bloc stained with 2% uranyl acetate, rinsed and dehydrated through a graded series of alcohols, and embedded with Eponate resin (Ted Pella, Redding, CA) at the University of Washington Pathology Electron Microscopy Resource Center. Next, the solid resin with embedded cells on gold electrode was peeled off the supporting plastic of the ECIS device. Sections of the resin were cut for TEM on a Reichert Ultracut E microtome device, mounted on 0.25% Formvar coated rhodium/copper grids, stained with uranyl acetate and lead citrate, and examined using a JEM 1200EX II transmission electron microscope (JEOL, Ltd., Tokyo) at an accelerating voltage of 80kV. A 1200 dpi resolution electronic copy of the TEM image was scanned from the negative film.

RESULTS AND DISCUSSION

The Concept of ECIS for Measuring Properties of an Individual Adherent Cell. Although there is a vast amount of literature on how to use ECIS to measure properties of a monolayer of cells,[27,33,39] we have not found any literature on how to use ECIS to measure h and A_{cell} of an individual cell. Figure

(37) Asami, K. *J. Non-Cryst. Solids* **2002**, *305*, 268–277.

(38) Krulevitch, P.; Ackler, H. D.; Becker, F.; Boser, B. E.; Eldredge, A. B.; Fuller, C. K.; Gascoyne, P. R. C.; Hamilton, J. K.; Swierkowski, S. P.; Wang, X.-B. U.S. Patent 6,437,551, 2002.

(39) Lo, C.-M.; Ferrier, J. *Phys. Rev. E* **1998**, *57*, 6982–6987.

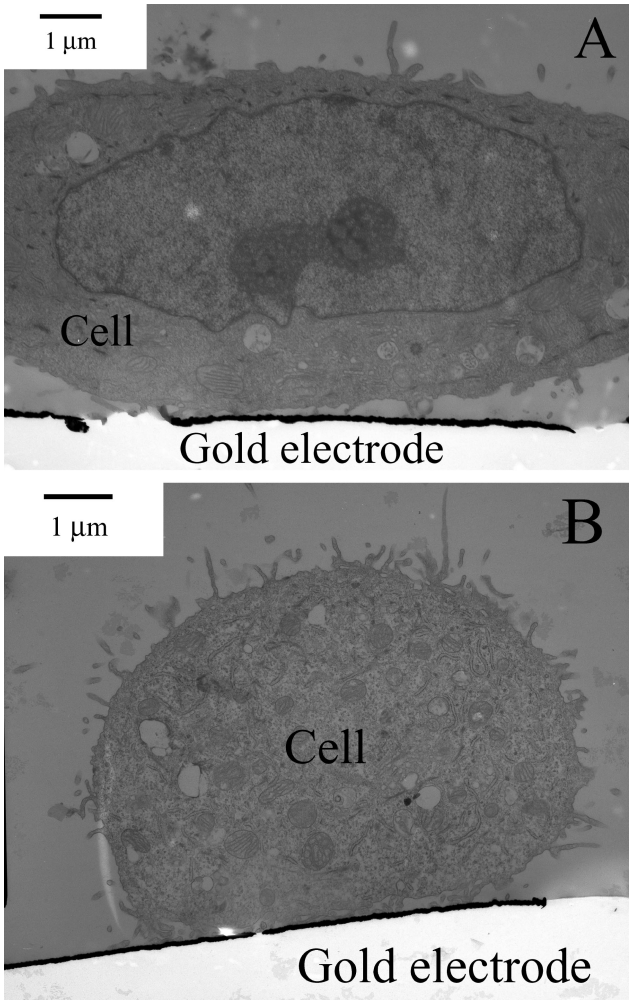

Figure 3. TEM image showing a cross section of an individual JEBG cell sitting on the gold electrode when (A) the cell was cut through the nucleus and (B) not cut through the nucleus. *h* varied along the basal membrane of the cell from less than 100 nm up to hundreds of nanometers. The *h* value obtained from the ECIS measurement fell within this range.

1A explains the concept of using the ECIS technique to measure properties of an individual cell. Several key differences have been observed between this work and the conventional ECIS associated with a monolayer of cells. The first difference was that the properties of the cell obtained from this measurement were those of one individual cell, not the average among all cells in the monolayer.

A second difference involved the microelectrode, which was designed to be as close to the dimension of the cell as possible so that a large change in impedance due to changes in h and A_{cell} of the individual cell or the highest signal-to-noise ratio was obtained.[40] Thus, the area of the microelectrode used in this study was 100 times smaller than that of the conventional ECIS. This smaller microelectrode, compared with the conventional microelectrode, resulted in (1) a higher Mag$Z(\omega)$ value and (2) a higher peak frequency (PF).[29] PF is the frequency where the change in Mag$Z(\omega)$ due to changes in h and A_{cell} is maximum. From the measurement of $Z(\omega)$, PF was around 100 kHz and Mag$Z(\omega)$ was

(40) Giaever, I.; Keese, C. R. *Proc. Natl. Acad. Sci. U.S.A.* **1984**, *81*, 3761–3764.

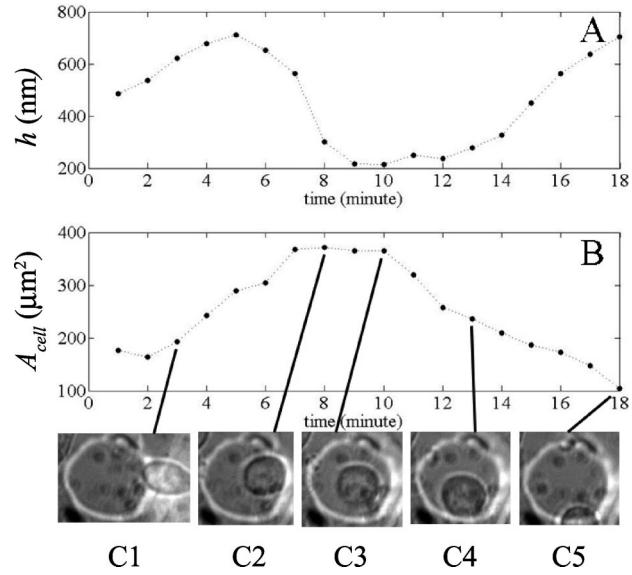

Figure 4. Time series of (A) h and (B) A_{cell} obtained from ECIS measurement when one individual JEBG cell moved in and out of the microelectrode in an 18 min period. (C) Snapshots of the cell over 18 min: (C1−C2) the cell was entering the electrode; (C3) the cell was completely inside the electrode; (C4) the cell was leaving the electrode; (C5) the cell had almost left the electrode.

about 100 times higher than that of the conventional ECIS. Knowing the value of PF was useful because the frequency range of the measurement was set around PF to minimize the i value used for each $Z(\omega)$.

A third difference involved the need to take into account the parasitic impedance that conducted leaky current elsewhere in the ECIS device. With conventional ECIS, the parasitic impedance was much higher than the main impedance, and thus it was neglected. In this case, however, because of the higher magnitude of impedance in the main current path due to the smaller microelectrode, the main impedance and the parasitic impedance became comparable and the effect of the parasitic impedance could not be ignored. Note that the parasitic impedance was represented by R_{para}, C_{para}, and C_{wire} and the main impedance was represented by Z_c, Z_{nc}, and R_s in the equivalent circuit model, respectively (Figure 1B).

Extraction of h and A_{cell} from $Z_{cell}(\omega)$. Figure 2A,B,C present the quality of fitting $Z_{cell}(\omega)$ using the equivalent circuit model developed. Figure 2A highlights a unique pair of h and A_{cell} values that gave the lowest S value equal to 0.0045 to obtain the best fit for $Z_{cell}(\omega)$ in both magnitude (Figure 2B1) and phase (Figure 2B2). The difference between $Z_{cell}(\omega)$ and $Z(\omega, h, A_{cell})$ was within 1% for the range of frequency used (Figure 2C). The h value of the individual JEBG cell (Figure 2D) obtained was 361 nm, whereas the value of A_{cell} obtained was 375 μm^2. Values of ρ, R_s, R_{para}, C_{para}, C_i, and α used in the model were 0.625 Ω·m, 10365 Ω, 198.75 Ω, 113 pF, 0.316 F/m^2, and 0.88, respectively.

The value of h obtained from $Z_{cell}(\omega)$ was well within the expected bounds (a few nanometers up to 4 μm); the upper bound was the height of the photoresist around the edge of the microelectrode (Figure 1A), and the lower bound was the lowest h value reported in the literature.[2,10,13,14,27,39] Also, the value of h fell within the submicron range in agreement with the range of h approximated from TEM images (Figure 3). Note that h obtained from TEM was only a rough estimate of the true value of h since

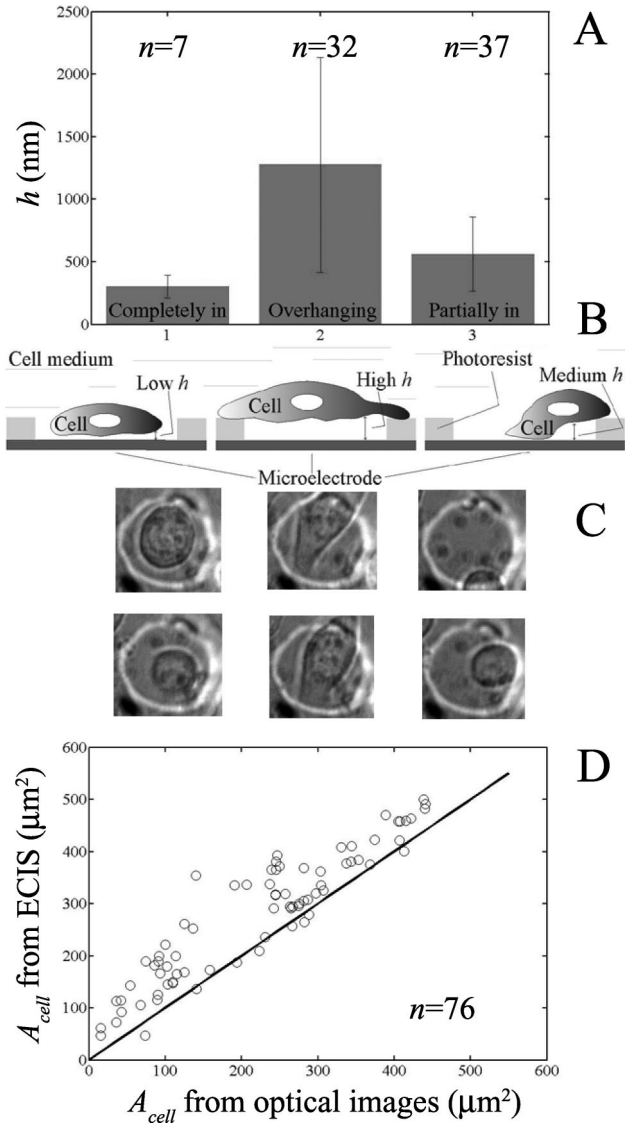

Figure 5. (A) Comparison of *h* obtained from ECIS among three groups categorized optically (error bar is 1 standard deviation). (B) The schematic views of the cell and microelectrode among three groups of *h*. The first group of *h* corresponded to a cell that was fully inside and attached well to the microelectrode. These *h* values were low and ranged from a few (the lower bound) up to a few hundreds of nanometers. The second group of *h* or high *h* corresponded to a cell that was completely overhanging between the opposite edges of the microelectrode made from a photoresist that was 4 μm high. The cell would not be able to attach well to the microelectrode, resulting in high values of *h* ranging from a few hundred nanometers up to 4 μm. The last group of *h* or medium *h* referred to a cell that was partially inside the microelectrode or overhanging from one edge of the microelectrode. Special cases of this group were obtained when the cell was descending into the microelectrode or leaving the electrode. Medium *h* values were somewhere in the middle between a few nanometers up to 4 μm. (C) A few examples of corresponding optical images among three groups of *h* were placed underneath each group of *h*. (D) Comparison of A_{cell} values between those obtained from ECIS and from optical measurements. The slope of this plot was close to 1 (solid line). For all plots, *n* is the number of data sets used in each plot.

(1) TEM was not a live cell measurement, (2) TEM images show *h* from cross sections of the cell, not *h* from the whole cell, and (3) the true *h* value could be altered in some degree by the preparation of TEM images. The value of A_{cell} obtained from $Z_{cell}(\omega)$ was very close to that of A_{cell} measured optically (368 ± 20 μm^2; average of three image processings) and well within the expected bounds (zero up to the measured value of $A_{microelectrode}$ = 716 μm^2). Although the normalized residuals were within 1% for all frequencies, which implied a good fit (Figure 2C), a clear trace around the horizontal axis suggested an imperfect match between the data and the model according to Boukamp.[32] In this work, however, the mismatch was not significant since both *h* and A_{cell} values were well within the expected ranges.

It should be noted that this work used Mag$Z(\omega)$ and phase$Z(\omega)$ to compute *S*, unlike the cases in the existing literature[32,41,42] where the real (Re$Z(\omega)$) and imaginary (Imag$Z(\omega)$) parts of $Z(\omega)$ were used. For some data sets, a smaller value of *S* indicating a smaller fitting error was obtained when using Mag$Z(\omega)$ and phase$Z(\omega)$ than using Re$Z(\omega)$ and Imag$Z(\omega)$. For other data sets, the values of *h* and A_{cell} as well as the value of *S* obtained from both computations were comparable. Also, in eq 1, the difference between $Z_{cell}(\omega)$ and $Z(\omega, h, A_{cell})$ was normalized using Mag$Z(\omega, h, A_{cell})$ and phase$Z(\omega, h, A_{cell})$. The normalization was necessary because of the large difference between the scales of the magnitude (10^3 to 10^5 Ω) and the phase (−90° to −75°) of the impedance spectrum (Figure 2B). Without this normalization, both Mag$Z(\omega)$ and phase$Z(\omega)$ could not be fit at the same time.

A Time Measurement of *h* and A_{cell} Using ECIS to Follow One Individual Cell. Eighteen impedance spectra were recorded continuously, and *h* and A_{cell} values were extracted (Figure 4A,B). All *h* and A_{cell} values were well within the expected bounds. The changes in *h* and A_{cell} with time were in agreement with the corresponding optical images (Figure 4C). The low values of *h* from minute 8 to minute 13 corresponded to the images of the cell sitting fully inside the microelectrode, allowing a small separation between the cell and the substrate (Figure 4 parts C2−C4). The values of *h* were higher at other time points because the cell was partially associated with the edge of the microelectrode and could not attach well to the substrate. Also, the increase in A_{cell} value from minute 1 to minute 7 and the decrease from minute 14 to 18 matched with the optical images of the cell while the cell was entering and leaving the microelectrode (Figure 4 parts C1 and C5). The global minimum of *S* was obtained for all 18 data sets, and the lowest values of *S* ranged from 0.0021 to 0.013. Values of ρ, R_s, R_{para}, C_{para}, C_i, and α used in the model were 0.632 Ω·m, 10459 Ω, 197.09 Ω, 114 pF, 0.296 F/m^2, and 0.893, respectively.

There was no limit on the measurement duration, and several thousand impedance spectra were easily handled in the data analysis. The custom impedance sensing setup allowed us to record $Z(\omega)$ and the corresponding optical image as often as one recording every 30 s. However, the length of the time series of *h* and A_{cell} reported here was limited by the behavior of the cell. For example, in Figure 4, the cell was spending only 18 min on the microelectrode, and thus the time series was 18 min long. As of now, we have not controlled or restricted how long the individual cell interacted with the substrate (a microelectrode). All data presented here were a representation of natural behavior of the cell without any stimuli in the setup.

(41) James Ross Macdonald. http://jrossmacdonald.com (accessed Nov 27, 2007).
(42) Bondarenko, A. S.; Ragoisha, G. A. EIS Spectrum Analyser. http://www.abc.chemistry.bsu.by/vi/analyser/ (accessed Nov 27, 2007).

Comparison of h and A_{cell} Obtained from ECIS and from Optical Microscopy. Although h could not be directly measured from optical images taken in the experiment, the values of h could be approximated from the images and categorized into three groups (Figure 5B). Figure 5A,B,C display good agreement between the values of h obtained from this electrical technique and the predicted values of h obtained from optical images. The mean value of h obtained from ECIS in the first group was 302 nm and lowest among the three groups, as expected. The mean of h in the second group was 1276 nm and the highest among the three groups, as expected, although they were not as high as 4 μm. This case applied when the cell was suspended and not stretching out very tightly between the opposite edges of the microelectrode. In the third group, the mean of h was 561 nm and stayed between the values in the first and second groups, as expected.

Figure 5D shows good agreement between A_{cell} values of the same data sets obtained from ECIS and from optical images. The minimum value of A_{cell} detectable from our technique was around 50 μm^2. The dynamic range was 1 order of magnitude (50−500 μm^2). The resolution was approximately 100 μm^2. A slight shift to the left, away from the ideal line that represented a linear relationship between A_{cell} values obtained from ECIS and from optical measurements, of some data, implied that some A_{cell} values obtained optically were lower than those obtained from ECIS. This lower than expected value of A_{cell} occurred because in some optical images, the edge of the individual cell could not be clearly distinguished from the background, especially when the edge of the cell was very thin. This could be improved by providing more uniform lighting and further minimizing any vibration in the setup. Also, it should be noted that all seven values of A_{cell}, when the cell was fully inside the microelectrode, were similar to A_{cell} values of individual JEBG cells grown on a tissue culture flask (data not shown). This finding indicated resembling surrounding conditions when a cell was either on a gold microelectrode or on a tissue culture flask.

CONCLUSIONS

This research demonstrates that two properties (the cell−substrate separation and the projected area) of an individual living cell could be obtained using an electrical method (ECIS). Learning how values of these properties are determined by a cell will shed light on the relationship between the cell and the substrate. This understanding is significant in the area of biomaterials, tissue formation, and cell biology. Measuring two properties with time has implications in the study of dynamic cellular processes, especially in cell adhesion and cell spreading. The advantage of this approach is that it enables measurements of properties of many individual cells in parallel. This will be a great benefit to the study of heterogeneity in cell populations and will help in the understanding of diseases such as cancer where phenotypically variable cells are present. This research also extends the sensitivity of the ECIS technique down to the individual cell level compared with the existing method of measuring properties of monolayers of cells. This will stimulate many new ideas for ECIS applications by researchers who have already become familiar with the conventional ECIS technique. The ECIS technique presented here not only can be used as a stand alone system but it also can be integrated with other sensing techniques such as optical microscopy to allow more probing of the individual cell. Thus, this effort can also be viewed as a development toward a commercial platform for measuring several properties of many individual living cells simultaneously.[43]

Several key developments still need to be integrated to push this technology toward a commercial platform. They include (1) the detailed characterization of the ECIS sensor, (2) the development of an array-based ECIS system, (3) the development of circuitry for parallel measurements of many individual cells, (4) the development of fully automated manipulation of individual cells on the sensing array, and (5) the development of real-time data analysis and display.

ACKNOWLEDGMENT

This work was supported by a grant from the NIH (P50 HG 002360). The JEBG cells were a gift from W. G. Carter (Fred Hutchinson Cancer Research Center, Seattle, WA). We thank Tim Ren and Steven Gales (Microsoft Corporation, Redmond, WA) for writing all the codes in *Capture*. We also thank Steve MacFarlane and Stephanie Lara for the TEM images.

Received for review January 7, 2008. Accepted March 10, 2008.

AC800036C

(43) Microscale Life Sciences Center. http://www.lifeonachip.org (accessed Dec 7, 2007).